UCLA

UCLA Previously Published Works

Title

A wireless patch for the monitoring of C-reactive protein in sweat

Permalink

https://escholarship.org/uc/item/5mq5v6ss

Journal

Nature Biomedical Engineering, 7(10)

ISSN

2157-846X

Authors

Tu, Jiaobing

Min, Jihong

Song, Yu

et al.

Publication Date

2023-10-01

DOI

10.1038/s41551-023-01059-5

Peer reviewed

eScholarship.org Powered by the California Digital Library
University of California

Author Manuscript

Author Manuscript

Author Manuscript

Author Manuscript

HHS Public Access

Author manuscript

Nat Biomed Eng. Author manuscript; available in PMC 2024 January 01.

Published in final edited form as:

Nat Biomed Eng. 2023 October ; 7(10): 1293–1306. doi:10.1038/s41551-023-01059-5.

A wireless patch for the monitoring of C-reactive protein in sweat

Jiaobing Tu[1], **Jihong Min**[1], **Yu Song**[1], **Changhao Xu**[1], **Jiahong Li**[1], **Jeff Moore**[2], **Justin Hanson**[3], **Erin Hu**[3], **Tanyalak Parimon**[4], **Ting-Yu Wang**[5], **Elham Davoodi**[1], **Tsui-Fen Chou**[5], **Peter Chen**[4], **Jeffrey J. Hsu**[3], **Harry B. Rossiter**[2], **Wei Gao**[1,*]

[1]Andrew and Peggy Cherng Department of Medical Engineering, Division of Engineering and Applied Science, California Institute of Technology, Pasadena, CA 91125, USA.

[2]Division of Respiratory and Critical Care Physiology and Medicine, The Lundquist Institute for Biomedical Innovation at Harbor-UCLA Medical Center, Torrance, CA 90502, USA.

[3]Division of Cardiology, University of California, Los Angeles, Los Angeles, CA, 90095, USA.

[4]Department of Medicine, Women's Guild Lung Institute, Cedars-Sinai Medical Center, Los Angeles, CA, 90048, USA.

[5]Proteome Exploration Laboratory, Beckman Institute, California Institute of Technology, Pasadena, CA, 91125, USA

Abstract

The quantification of protein biomarkers in blood at picomolar-level sensitivity requires labour-intensive incubation and washing steps. Sensing proteins in sweat, which would allow for point-of-care monitoring, is hindered by the typically large interpersonal and intrapersonal variations of the sweat matrix. Here, we report the design and performance of a wearable and wireless patch for the real-time electrochemical detection of the inflammatory biomarker C-reactive (CRP) protein in sweat. The device integrates iontophoretic sweat extraction, microfluidic channels for sweat sampling and for reagent routing and replacement, and a graphene-based sensor array for quantifying CRP (via an electrode functionalized with gold-nanoparticle-conjugated anti-CRP capture antibodies), as well as ionic strength, pH and temperature, for the real-calibration of the CRP sensor. In patients with chronic obstructive pulmonary disease, with active or past infections, or who had heart failure, the elevated concentrations of CRP measured via the patch correlated

Reprints and permissions information is available at www.nature.com/reprints.

[*]**Correspondence and requests for materials** should be addressed to weigao@caltech.edu.

Author contributions

W.G., and J.T. initiated the concept and designed the overall studies; W.G. supervised the work; J.T., J.M., and Y.S. led the experiments and collected the overall data; C.X., J.L., T.W., E.D., and T.C. contributed to sensor characterization and validation; J.M., J.H., E.H., T.P., P.C., J.J.H., and H.B.R. contributed to the design of the human trials and system evaluation in human subjects. All authors contributed the data analysis and provided feedback on the manuscript.

Competing interests

The authors declare no competing interests.

Extended data is available for this paper at https://doi.org/10.1038/s41551-02X-XXXX-X.

Supplementary information The online version contains supplementary material available at https://doi.org/10.1038/s41551-02X-XXXX-X.

Author Manuscript Author Manuscript Author Manuscript Author Manuscript

well with the protein's levels in serum. Wearable biosensors for the real-time sensitive analysis of inflammatory proteins in sweat may facilitate the management of chronic diseases.

One-sentence editorial summary :

A wearable electrochemical patch for the real-time monitoring of the biomarker C-reactive protein in sweat detects elevated concentrations of the protein in patients with acute or chronic inflammation.

Inflammatory processes and immune responses are associated with a broad spectrum of physical and mental disorders that contribute substantially to modern morbidity and mortality globally. The top three leading causes of death worldwide, namely, ischemic heart disease, stroke, and chronic obstructive pulmonary disease (COPD), are each characterized by chronic inflammation[1–3]. Although the acute inflammatory response is a critical survival mechanism, chronic inflammation contributes to long-term silent progression of disease through irreversible tissue damage[4–6]. Delayed diagnosis and treatment of chronic diseases impose heavy financial burdens on patients and the healthcare systems[2,4]. A readily available means of monitoring inflammatory biomarkers at home could improve patient outcomes and lower cost factors by monitoring disease progression and initiating early treatment and intervention[7].

Although there is no canonical standard biomarker for the measurement and prediction of systemic chronic inflammation6, C-reactive protein (CRP), an acute-phase protein synthesized by hepatocytes in response to a wide range of both acute and chronic stimuli, has a close association with chronic inflammation and respective risks of mortality in several disease states (Fig. 1a)[8–12]. The stable nature of CRP in plasma, the absence of circadian variation, and its insensitivity to common medications such as corticosteroids render it extremely attractive to clinicians as a handy means to assess a patient's physiological inflammatory state[13]. There is also a growing interest in exploring the effectiveness of serial CRP measurements for therapeutic decision-making[14,15].

At present, circulating CRP levels are clinically assessed in specific laboratories that rely on invasive blood draws from patients (Supplementary Table 1). Commercial point-of-care CRP monitors are still bulky in size and cannot reach picomolar-level sensitivity to assess CRP levels in non-invasively accessible alternative biofluids such as sweat and saliva (Supplementary Table 2). A faster, sensitive, non-invasive, and user-friendly approach, accessible to not only clinicians but also patients and caregivers, could unleash the full potential of inflammatory biomarker monitoring for clinical management beyond hospital settings.

Recent advances in flexible electronics and digital health have transformed conventional laboratory tests into remote wearable molecular sensing that enables real-time monitoring of physiological biomarkers[16–24]. Sweat contains abundant biochemical molecules ranging from electrolytes and metabolites, to large proteins[25,26], and importantly, it is readily accessible by non-invasive techniques (Fig. 1a). However, currently reported wearable biosensors are largely restricted to the detection of a limited selection of biomarkers

Author Manuscript Author Manuscript Author Manuscript Author Manuscript

such as electrolytes and metabolites at μM or greater concentrations via ion-selective and enzymatic sensors or direct oxidation/reduction[16,20,27–40]. The majority of clinically relevant protein biomarkers including CRP are present at nM to pM levels in blood while the anticipated levels of proteins in sweat are expected to be much lower than in blood[26]. Despite recent efforts in the development of wearable bioaffinity biosensors for trace-level biomarkers such as cortisol, the accurate and in situ detection of sweat protein biomarkers remains a major challenge due to their extremely low concentrations (pM level) and the large interpersonal and intrapersonal variations in sweat compositions[41–44]. The detection of protein biomarkers usually requires integrating bioaffinity receptors such as antibodies and aptamers[43,45]. However, such techniques typically require lengthy target incubation, labour-intensive washing steps, and the addition of redox solutions for signal transduction. Thus, there is a strong desire for a wearable biosensing technology that allows automatic in situ monitoring of ultra-low-level circulating proteins at home and in community settings.

In this work, we report a wireless wearable nanobiosensor, InflaStat, for non-invasive personalized inflammatory status monitoring (Fig. 1b–e). It consists of an autonomous iontophoresis module for on-demand and controlled sweat extraction, a sweat gland-powered skin-interfaced microfluidic module that capitalizes on sweat flow to achieve fully automated protein and detector antibody capturing, subsequent washing, and picomolar-level electrochemical detection on the skin, and a flexible nanoengineered multiplexed sensor array for in situ sweat inflammatory biomarker analysis. The use of gold nanoparticles (AuNPs)-decorated mass-producible laser-engraved graphene (LEG) enables highly sensitive and efficient electrochemical detection of trace-level sweat CRP in situ on the skin. AuNPs conjugated with electroactive redox molecule thionine (TH) and detector antibody (dAb) enable efficient electrochemical signal transduction (Signal ON) and further signal amplification. The integrated pH, temperature, and ionic strength graphene sensors enable real-time personalized CRP data calibration to mitigate the interpersonal sample matrix variation-induced sensing error, and provide a more comprehensive assessment of the inflammatory status[46,47]. We confirmed the presence of CRP in human sweat from healthy subjects and identified elevated sweat CRP levels in patients with chronic and acute inflammations associated with COPD, heart failure (HF), and active and past infections (e.g., COVID-19). A strong correlation between sweat and serum CRP levels was obtained in both healthy and patient populations, indicating the utility of this technology in non-invasive disease classification, monitoring, and management.

Results & Discussion

Design of the wearable microfluidic LEG-AuNPs biosensor.

Key components of the wearable sensor are a skin-interfaced flexible, disposable, multiplexed microfluidic biosensor patch fabricated on a polyimide (PI) substrate via CO_2 laser engraving and a flexible printed circuit board (FPCB) for iontophoretic sweat induction, sensor data acquisition and wireless communication (Fig. 1b and Supplementary Fig. 1). The sensor array consists of an electrodeposited AuNPs-decorated LEG working electrode immobilized with anti-CRP capture antibodies (cAb), a Ag/AgCl reference electrode, an LEG counter electrode for sweat CRP capturing and electrochemical

Author Manuscript Author Manuscript Author Manuscript Author Manuscript

analysis, an LEG-based impedimetric ionic strength sensor, a LEG-polyaniline-based potentiometric sweat pH sensor, and a strain-insensitive resistive graphene temperature sensor (Supplementary Fig. 2). Considering that the potential users of this technology include sedentary and immobile patients, an iontophoresis module (based on a pair of LEG electrodes) is incorporated for on-demand delivery of cholinergic agonist carbachol from the carbachol hydrogel (carbagel) for autonomous sweat stimulation throughout daily activities without the need for vigorous exercise. A cost-effective and flexible microfluidic module is assembled by stacking laser-cut medical adhesives and polyethylene terephthalate (PET) for efficient sweat sampling (Fig. 1c). The miniaturized FPCB interfaces compactly on top of the microfluidic sensor patch to form the fully integrated wearable system (Fig. 1d). Powered by a small on-board lithium battery, the wearable system is able to wirelessly communicate with a user interface via Bluetooth Low Energy (Supplementary Fig. 3).

In order to realize automatic wearable CRP detection in situ, the microfluidic module comprises a reagent reservoir for the storage of the labeled anti-CRP dAbs-conjugated AuNPs, a serpentine mixing channel for mixing of dAb with sweat CRP, and a detection reservoir for the capture and quantification of sweat CRP (Fig. 1e and Supplementary Video 1). The redox molecule, TH, is used to label the nanoparticle conjugates to achieve direct electrochemical sensing. As the autonomously induced sweat flows into the microfluidics, the deposited dAbs conjugated AuNPs are reconstituted within the reagent reservoir (I) and routed along with sweat through a serpentine passive mixer to facilitate the dynamic binding between sweat CRP and dAb (II). As the mixture enters the detection reservoir, it slowly fills the chamber before exiting via the outlet; the detection reservoir has an optimized size to allow sufficient time for CRP-dAb to bind with anti-CRP cAb functionalized LEG-AuNPs working electrode (III). Subsequently, a fresh sweat stream continues to refresh the microfluidics to achieve passive label removal (IV). Square wave voltammetry (SWV) is used to measure the amount of TH bound to the working electrode surface. Since TH molecules are directly conjugated to CRP dAb-immobilized AuNPs, their amount bound is directly correlated to the amount of CRP ‘sandwiched’ between cAbs at the electrode surface and dAb-immobilized AuNPs, and consequently, the initial concentration of CRP in solution.

Materials and electrochemical characterizations of the LEG-AuNPs immunosensor.

The functionalization process for the preparation of the CRP immunosensor is illustrated in Fig. 2a and Supplementary Fig. 4. AuNPs are electrodeposited on the LEG surface followed by subsequent thiol monolayer assembly with mercaptoundecanoic acid and mercaptohexanol. As the formation of SAM layer relies on specific gold-sulfur bonding, immersion of the sensor patch in alkanethiol solution has negligible influence on other graphene-based electrodes (Supplementary Fig. 5). Pulsed potential-deposited AuNPs evenly distribute throughout the mesoporous graphene structure and possess superior electrocatalysis capability and form a large number of binding sites on the surface of the particles for biomolecule immobilization (Fig. 2b,c and Supplementary Fig. 2b). This substantially improves the sensitivity of the CRP sensor with little non-specific adsorption (Supplementary Fig. 6). The formation of LEG-AuNPs composite is confirmed through the increased ratio of the intensity of D and G bands in the Raman spectra due to the presence

Author Manuscript Author Manuscript Author Manuscript Author Manuscript

of AuNPs (Fig. 2d)[48]. The individual sensor modification steps on the LEG electrodes are characterized with X-ray photoelectron spectroscopy (Fig. 2e and Supplementary Fig. 7). The intensity of Au4f increases substantially after the deposition of AuNPs while N1s increases only after the cAb immobilization step, indicating successful electrode preparation (Fig. 2e). Differential pulse voltammetry (DPV) and electrochemical impedance spectroscopy (EIS) were used to further characterize the LEG surface electrochemically after each modification step (Fig. 2f and Supplementary Fig. 8). The decrease in peak current height in DPV voltammograms and increased resistance in Nyquist plots after self-assembled monolayer (SAM) and cAb protein immobilization indicate that SAM and cAb impede the electron transfer at the interface. This is due to the increase in surface coverage by non-conductive species. Moreover, the negatively charged carboxylate functional groups in the SAM layer result in the repulsion of the negatively charged redox indicator, ferricyanide, and further reduces the electron transfer rate. Subsequent modification of the SAM layer with EDC/NHS chemistry replaces the negatively charged carboxylate groups with neutral NHS-ester groups. This is empirically observed as an increase in peak current height. Such electrode fabrication processes show high batch-to-batch reproducibility as the main processes including laser engraving, electrochemical deposition, and solution process are all mass-producible (Supplementary Fig. 9).

In order to realize trace-level sweat CRP analysis, PEGylated AuNPs that possess large surface area-to-volume ratio are functionalized with polystreptavidin R to increase the loading of biotinylated-dAbs and subsequently enhance the sensitivity (Supplementary Figs. 10 and 11). One-step direct electrochemical detection is enabled by crosslinking the redox label TH onto the carboxylate residues on the dAb-loaded AuNPs. As the TH-labelled dAb-loaded AuNPs bind to the mesoporous graphene electrode upon CRP recognition, TH located on the external sites of the proteins are in close proximity to the graphene surface in each mesopores for electron transfer. Increases in hydrodynamic sizes (Fig. 2g) and the shifts of ultraviolet-visible (UV-Vis) absorbance (Supplementary Fig. 12) of the AuNPs conjugate after each modification step, along with the transmission electron microscope (TEM) image of the dispersed AuNPs-dAb conjugates (Fig. 2h) confirm the successful immobilization of the dAbs.

The performance of the CRP sensor was evaluated with SWV in CRP spiked phosphate-buffered saline (PBS) solutions (Fig. 2i). The increases in peak current height of TH reduction show a linear relationship with increased target concentrations (Fig. 2j). The sensor showed an ultralow limit of detection of 8 pM, good batch-to-batch reproducibility (Supplementary Fig. 13), and the sensing accuracy can be further enhanced by automating the sensor preparation and modification process (e.g., *via* automated fluid dispensing or inkjet printing[49]). The LEG-AuNPs CRP immunosensor demonstrates high selectivity over other potential interference proteins and hormones attributed to the sandwich assay format (Fig. 2k and Supplementary Fig. 14). Considering interpersonal variations during the human study, the influence of sweat pH, ionic strength, temperature, and sample volume on the antibody-antigen binding kinetics and redox probe electron transfer rate on CRP sensing accuracy was investigated (Supplementary Fig. 15) and mitigated by introducing suitable calibration mechanisms. The potential variations of the Ag/AgCl pseudo-reference electrode in the presence of varying Cl^- concentration in the physiologically-relevant range result

Author Manuscript Author Manuscript Author Manuscript Author Manuscript

in a small shift in the peak potential but its influence on the overall peak current density (and thus CRP quantification) is negligible (Supplementary Fig. 16). The accuracy of the CRP sensor for biofluid analysis was validated by the laboratory gold standard enzyme-linked immunosorbent assay (ELISA) using human sweat and saliva samples (Fig. 2l). The disposable CRP sensors also maintained stable sensor performance over a 10-day period when stored in PBS in the refrigerator at 4°C (Supplementary Fig. 17).

Evaluation of sweat CRP for non-invasive monitoring of systemic inflammation.

Despite the high potential of non-invasive CRP monitoring, the presence and levels of CRP in sweat are extremely underexplored in the literature[50]. To affirm the presence of CRP in sweat generated by iontophoresis and by vigorous exercise, we first conducted a proteomic characterization of different types of sweat samples using bottom-up proteomic analysis as illustrated in Fig. 3a. Using a recombinant CRP protein standard as the reference, we identified CRP in both exercise and iontophoretic sweat samples from human subjects (Fig. 3b, Supplementary Fig. 18, and Supplementary Table 3). In this regard, we further evaluated the use of our LEG-AuNPs CRP sensors for the assessment of sweat CRP as a universal, cost-effective, and non-invasive approach to monitor systemic inflammation in various disease states (Fig. 3c and Supplementary Tables 4–6).

We investigated healthy subjects grouped according to smoking status (current, former, and never smokers), where CRP levels in both serum and sweat were greater in current smokers as compared with former and never smokers (Fig. 3d), consistent with previous reports on the effect of current smoking on serum CRP[51]. However, among COPD patients, serum and sweat CRP values were greater in former smokers than current smokers, consistent with irreversible tissue damage and chronic inflammation in COPD patients even after smoking cessation[52]. Monitoring sweat CRP in COPD patients may therefore be useful for following disease progression and/or predicting exacerbation in this patient population[53].

Chronic systemic inflammation is also related to increased risks of cardiovascular events[3]. In a preliminary study with HF patients, our sensor results show that serum and sweat CRP values were substantially elevated in HF patients with preserved ejection fraction (HFpEF) but not in HF patients with reduced ejection fraction (HFrEF) (Fig. 3e), consistent with past studies[54–57]. The investigation of the dynamics of sweat CRP using our technology could potentially have high value in predicting HFpEF disease progression and clinical outcomes[55].

In addition to chronic infections in COPD and HF, it is well known that acute infections (such as COVID-19) could lead to severe inflammatory responses[14]. In a pilot study, we evaluated our sensor on hospitalized patients with active infections for two consecutive days (Fig. 3f). Substantial increase (over 10-fold on average) in both serum and sweat CRPs was identified in patients with active infection as compared with healthy subjects, indicating the presence of highly elevated sweat CRP in acute inflammation.

By analysing the samples from healthy subjects and patient populations with various inflammatory conditions using our sensor, a high correlation coefficient (r) of 0.844 (n=80) between sweat and serum CRP concentrations was obtained (Fig. 3g). Such correlation

Author Manuscript Author Manuscript Author Manuscript Author Manuscript

appears to be higher than those obtained from saliva and urine samples (Supplementary Fig. 19), suggesting the great potential of using sweat CRP for the non-invasive monitoring of systemic inflammation toward the management of a variety of chronic and acute health conditions.

Characterization of the multiplexed microfluidic patch for automatic immunosensing.

In order to realize accurate and automatic immunosensing *in situ*, the flexible sensor patch was designed to have a laser-engraved microfluidic module (consisting of a reagent reservoir, a mixing channel, and a detection reservoir) and a multiplexed LEG sensor array (consisting of a CRP immunosensor, an ionic strength sensor, and a pH sensor) (Fig. 4a). As the microfluidic module routes sweat passively on the skin, the impedimetric ionic strength sensor automatically captures the state of the detection reservoir (reagent flow and refreshment); the measured admittance signals show a log-linear response with the electrolyte concentrations (Fig. 4b,c). As large interpersonal variations in electrolyte and pH levels were observed in both exercise and chemically induced sweat samples (Supplementary Fig. 20), high-level buffering salts were deposited with the dAbs in the reagent reservoir to mitigate potential binding environment changes caused by sweat composition variations (Supplementary Fig. 21). As such, this introduces an electrolyte gradient between the detection reagent reconstituted sweat (mixture) and fresh sweat that subsequently enters the detection reservoir. According to the numerical simulation, the routing of sweat and detection reagents can be summarized into four steps: reconstitution (I), incubation (II), refreshment (III), and detection (IV) (Fig. 4d,e and Supplementary Note 1). Based on the microfluidic flow test using artificial sweat (0.2X PBS) under a mean physiological sweat rate (1.5 μL min^{-1}), the admittance signal is close to zero initially when no fluid enters the chamber during the reconstitution stage; as reconstituted, high-salt loaded detection reagents flow into the detection chamber, admittance reaches its peak value and gradually decreases as high-salt loaded reagents are flushed out of the detection chamber by newly secreted sweat (Fig. 4f). Since electrolyte content in iontophoresis sweat remains relatively stable for the same individual[28], the admittance response plateaus after all reagents have been refreshed by natural sweat, indicating the working electrode is ready for electrochemical CRP detection. Further experimental flow test using fluorescent proteins (fluorescein isothiocyanate-albumin as CRP surrogate and peridinin chlorophyll protein as detection reagent) shows a similar trend in incubation and refreshment process as the simulation and electrolyte flow test (Fig. 4g and Supplementary Video 2). Based on sweat rate information collected from 24 current and former smokers with and without COPD (Supplementary Fig. 22), flow tests with flow rates varying from 0.5 to 3.5 μL min^{-1} show similar admittance patterns with plateaus after various refreshing processes (Fig. 4h). The gradient of admittance at different flow rates converges to zero, as pre-loaded salts and dye are refreshed from the detection reservoir. The mean sweat volume routed during this process before sensors readings were taken was estimated to be 21 μL based on flow rate and admittance measurements (Fig. 4h).

The performance of CRP sensors based on this automated electrolyte monitoring mechanism was evaluated in multiple microfluidic flow tests. SWV electrochemical measurements were initiated during the admittance plateaus (Fig. 4i). An increased concentration (from 1 to 5 ng

Author Manuscript Author Manuscript Author Manuscript Author Manuscript

mL^{-1}) led to an increased SWV peak current height while no substantial difference in CRP sensor response was observed for the same concentration under physiologically relevant flow rates (1, 1.5, 2.5, and 3.5 μL min^{-1}) (Fig. 4i,j and Supplementary Fig. 23). Although a higher flow rate could also result in a faster refreshment of the detection chamber and thus a shorter incubation time for the detection antibody and CRP, the increment in CRP signals under varying incubation time corresponding to the physiologically relevant sweat rates (between 5 and 20 minutes) is relatively small (Supplementary Fig. 15). Although the binding condition is pre-adjusted with deposited salts, the flow test with different initial electrolyte concentrations (0.1X and 0.2X PBS were chosen as artificial sweat to simulate interpersonal variations in sweat electrolyte concentrations) shows slightly decreased SWV signals at the lower electrolyte concentration due to the influence of electrolyte levels on the rate of TH reduction (Fig. 4k,l). Similar to *in vitro* selectivity results, no major interferences on the CRP detection signal were observed in the flow test (Supplementary Fig. 24). Moreover, flow tests using artificial sweat with different pH levels lead to varied SWV signals (Supplementary Fig. 25). These results indicate that sweat rate calibration is not necessary while additional *in situ* signal calibrations with sweat pH and electrolyte levels are needed to mitigate the interpersonal variations on CRP detection accuracy. Compared to previously reported passive wearable microfluidic sensors which rely on vigorous exercise to induce sweat and cannot reach sensitivities below mM levels (Supplementary Table 7), our technology offers an attractive fully automated microfluidic sweat induction, harvesting, and high-accuracy quantitative analysis solution, ideally suitable for at-home monitoring of clinically relevant trace-level biomarkers.

System integration and on-body evaluation of the wearable biosensor.

The fully integrated wearable inflammation monitoring system, InflaStat, is designed based on vertical stack assembly of a flexible microfluidic sensor patch and an FPCB and can be comfortably worn by the subjects (Fig. 5a). As illustrated in electronic circuit block diagram and schematic in Fig. 5b and Supplementary Fig. 26, the FPCB is able to perform current-controlled iontophoresis, multiplexed electrochemical measurements (including voltammetry, impedimetry, and potentiometry), signal processing, and wireless communication. The integrated system could also accurately obtain the dynamic responses of the integrated LEG-based pH, ionic strength, and skin temperature sensors for real-time CRP sensor calibration (Fig. 5c–f, Supplementary Fig. 27). The InflaStat is designed to have good mechanical flexibility and stability toward practical usage during various physical activities. Each individual sensor shows relatively small variations under a moderate radius of bending curvature (5 cm) (Supplementary Fig. 28). More strain-insensitive sensor designs can be included when necessary[58]. During on-body operation, the InflaStat can conformally adhere to the skin through medical adhesive with *in situ* CRP sensing performed in the microfluidics without direct sensor-skin contact.

Clinical on-body evaluation of the wearable system was performed on healthy subjects (involving both never smokers and current smokers) as well as patients with COPD and post-COVID-19 infection (Fig. 5g–l and Supplementary Fig. 29–31). During the on-body trials, the wearable system laminates conformally on the subject's arm, chemically induces and analyzes sweat (Supplementary Video 3 and Supplementary Fig. 32), and acquires

Author Manuscript Author Manuscript Author Manuscript Author Manuscript

inflammatory biomarker information non-invasively and wirelessly (Fig. 5g). The obtained sensor data can be displayed on a custom developed mobile app in real-time (Fig. 5h). *In situ* pH, temperature, and CRP sensor readings are acquired after the ionic strength sensor indicate full refreshment of the detection reservoir (Fig. 5h–l). It should be noted that the TH's reduction peak for the CRP sensor appears at a slightly shifted potential given the variations in sweat pH (Supplementary Fig. 33). The CRP concentration was converted in the mobile app based on the obtained SWV voltammogram and the corresponding real-time obtained ionic strength, pH, and temperature values (Supplementary Fig. 34 and Supplementary Note 2). As expected, an elevated CRP level was observed from the current smokers as compared with the never smokers in healthy subjects. The CRP levels in the COPD patients and post-COVID subjects were substantially greater than those of non-smoking healthy subjects, suggesting the promise of using the InflaStat in practical non-invasive systemic inflammation monitoring and disease management applications. *In vitro* analysis of sweat and serum from post-COVID subjects corroborate the on-body observation that patients who experienced moderate symptoms during COVID may still present a low-grade inflammation post COVID episode as indicated by the slightly elevated CRP levels (Supplementary Fig. 35 and Supplementary Table 8). It should be noted that similar as serum, sweat CRP levels remained stable during the test period (Supplementary Fig. 36) and no substantial variations were observed for chemically-induced sweat samples at different body locations (Supplementary Fig. 37).

Conclusion

We developed a fully integrated wearable biosensor patch for real-time, non-invasive inflammatory biomarker monitoring through automatic *in situ* microfluidic analysis. The wearable sensor is capable of autonomous sweat extraction, harvesting, biomarker analysis, and wireless data transmission in sedentary individuals on-demand across daily human activities. In contrast to previous wearable technologies for monitoring biomarkers and our previously reported LEG-based sensors which typically detects metabolites at μM or higher level[27,59], this technology realizes highly sensitive detection of ultra-low-level inflammatory proteins *in situ* with a 6 orders-of-magnitude (picomolar level) improvement in sensitivity through a holistic combination of 1) a nanoengineered immunosensor highly sensitive and selective CRP analysis, 2) a microfluidic module for automatic sweat extraction, sampling, reagent routing and refreshing, 3) and a multiplexed graphene sensor array for real-time data acquisition and sensor calibration. The operation principle proposed herein can be readily adapted to survey a broad array of inflammatory biomarkers (e.g., cytokines) and beyond. We assessed the elevation of sweat CRP in healthy subjects and patients with various health conditions (e.g., COPD, HF, and active and past infections) for the monitoring of chronic and acute systemic inflammation and reported a high correlation between sweat and serum CRP levels. In practice, the spot checking of CRP every several hours is sufficient to monitor active infections and immune responses. The disposable point-of-care CRP sensor patch design with a reusable wearable electronic system serves the purpose of immediate, non-invasive, on-the-skin assessment of circulating CRP at any given time. When necessary, dynamic and automatic wearable CRP sensing could be realized by incorporating capillary bursting valves[60] and CRP sensor arrays into a single disposable sensor patch. It is also

Author Manuscript Author Manuscript Author Manuscript Author Manuscript

worth noting that although the clinical use cases we demonstrate in this work do not conform to current clinical practices, the reason behind this disparity is the lack of such specific, immediate, and non-invasive inflammation assessment tools rather than the lack of needs. The current turnaround time (1 day) of the clinical high-sensitivity CRP Test (hsCRP) does not meet this need for frequent assessments. In addition to hospitalized cases which require close monitoring of inflammatory state, many chronic diseases, such as COPD and inflammatory bowel disease, could benefit from at-home, daily or frequent, fully automatic, and non-invasive assessment of CRP for disease management.

Outlook

This wearable technology provides quantitative, personalized inflammatory information that addresses the unmet needs of patients and caregivers of chronic inflammatory diseases as society progresses towards decentralized medicine. Furthermore, given sweat's accessibility and its non-invasiveness, it enables the interrogation of the dynamicity of CRP in various disease models and providing clinical insights previously unfathomable. Further investigation of the metabolic timeline of sweat CRP in response to inflammatory stimuli and therapy initiation may provide insight into its promptness in clinical diagnosis and decision-making. This wearable approach can be adapted to assess other trace-level disease-relevant protein biomarkers on-demand.

Methods

Materials and reagents.

Silver nitrate, iron chloride (III) and hydrogen tetrachloroaurate (III) hydrate were purchased from Alfa Aesar. Sodium thiosulfate pentahydrate, sodium bisulfite, 2-(N-morpholino)ethanesulfonic acid hydrate (MES), mercaptoundecanoic acid (MUA), mercaptohexanol (MCH), N-(3-Dimethylaminopropyl)-N'-ethylcarbodiimide (EDC), N-hydroxysulfosuccinimide sodium salt (sulfo-NHS), bovine serum albumin (BSA), hydroquinone, hydrocortisone, human immunoglobulin G (IgG), thionine acetate salt, Albumin–fluorescein isothiocyanate conjugate (FITC-albumin), 1H-Pyrrole-1-propionic acid (PPA), 1-Pyrenebutyric acid (PBA), Tween® 20, chloroacetamide,(4-(2-hydroxyethyl)-1-piperazineethanesulfonic acid (HEPES), calcium chloride, 3 kDa Amicon Ultra-0.5 centrifugal filter unit, and urea were purchased from Sigma Aldrich. Potassium ferricyanide (III), and potassium ferrocyanide (IV) were purchased from Acros Organics. Potassium chloride, 96-well Nunc MaxiSorp™ flat-bottom plate, Pierce™ Protein Concentrators PES, 100K MWCO, 0.5 mL, lyophilized human tumor necrosis factor alpha (TNF-α), trypsin, Pierce™ C18 Spin Columns were purchased from Thermo Fisher Scientific. Agarose, sulfuric acid, hydrochloric acid, sodium carbonate anhydrous, sodium bicarbonate, sodium chloride, sodium dihydrogen phosphate, potassium hydrogen phosphate, potassium chloride, hydrogen peroxide (30% (w/v)), dimethylformamide (DMF), LCMS grade acetonitrile, HPLC grade water, folic acid, trifluoroacetic acid, and 10X phosphate-buffered saline (PBS) were purchased from Fisher Scientific. 20 nm carboxyl (carboxyl-PEG3000-SH) gold nanoparticles (AuNPs) was purchased from Cytodiagnostics Inc. CRP capture antibody (cAb) and biotinylated detector antibody (dAb) were from

Author Manuscript Author Manuscript Author Manuscript Author Manuscript

the ELISA kit purchased from R&D systems (Human CRP DuoSet ELISA, DY1707). Recombinant human CRP protein standard was purchased from Abcam (ab167710). Medical adhesives were purchased from 3M and Adhesives Research. Polyimide (PI) films (75-μm thick) were purchased from DuPont. Polyethylene terephthalate (PET) films (50 μm thick) were purchased from McMaster-Carr. SureLight® Peridinin-Chlorophyll Protein Complex was purchased from Assaybio. Lysyl endopeptidase was purchased from FUJIFILM Wako Chemical Corp.

Fabrication of the multiplexed microfluidic sensor patch.

A PI film was raster engraved at focus height (8% Power, 15% Speed, 1000 Points Per Inch) to fabricate laser engraved graphene (LEG)-based iontophoresis (IP) electrodes, connection leads, impedance, CRP working, counter and reference electrodes using a 50 W CO_2 laser cutter (Universal Laser System). The pH electrode and temperature sensor were engraved using vector mode with 1% and 3% Power, respectively (15% Speed, 1000 Points Per Inch (PPI)). The working electrode of pH sensor was prepared by electrochemically cleaning the LEG electrode in 1M HCl via cyclic voltammetry from −0.2 to 1.2 V at 0.1V s^{-1} for 10 cycles followed by electrodeposition of polyaniline pH sensing membrane *via* cyclic voltammetry from −0.2 to 1.2 V at 0.1 V s^{-1} for 10 cycles. The shared Ag/AgCl reference electrode was fabricated by electrodeposition of Ag on the LEG electrode in a solution containing silver nitrate, sodium thiosulfate, and sodium bisulfite (250 mM, 750 mM, and 500 mM, respectively) using multi-current steps (30 s at −1 μA, 30 s at −5 μA, 30 s at −10 μA, 30 s at −50 μA, 30 s at −0.1 mA and 30 s at −0.2 mA), followed by drop casting 10 μL-aliquot of 0.1M iron chloride (III) for 1 minute. AuNPs were electrodeposited on the LEG CRP working electrode *via* pulse deposition (two 0.5 s pulses at −0.2 V separated by a 0.5 s pulse at 0 V) for 40 cycles in the presence of 0.1 mM gold(III) chloride trihydrate and 10 mM sulfuric acid.

The iontophoresis hydrogels containing cholinergic agent carbachol (placed on the IP electrodes) were prepared by dissolving agarose (3% w/w) in deionized water using a microwave oven. After the agarose was fully dissolved, the mixture was cooled down to 165 °C and 1% carbachol for anode (or 1% KCl for cathode) was added to the above mixture and stirred to homogeneity. The cooled mixture was casted into cylindrical molds or assembled microfluidic patch and solidified at room temperature. The hydrogels were stored at 4 °C until use.

To prepare the microfluidic module, an assembly of thin PET film (50 μm) sandwiched between double-sided medical adhesives (180 μm top layer, 260 μm bottom layer with a 50 μm PET backing) was attached to a substrate and cut through to make the channels and reagent reservoirs using the laser cutter at 2.7% power, 1.8% speed, 1000 PPI vector mode. Next 4% power, 10% speed, 1000 PPI vector mode was used to cut a circular outline through only the top layer of medical adhesive (180 μm). The circular top layer was peeled off to make the detection reservoir. A sweat accumulation layer was prepared by cutting through a 130 μm adhesive. The labeled dAb-AuNPs were drop-casted and dried in the reagent reservoir and stored in dry state at 4°C before assembly with the sensor patch.

Author Manuscript Author Manuscript Author Manuscript Author Manuscript

LEG-AuNPs CRP working electrode functionalization.

LEG-AuNPs working electrodes were immersed in 0.5 mM MUA and 1 mM MCH in proof 200 ethanol overnight for self-assembled monolayer (SAM) formation. After rinsing with ethanol followed by deionized (DI) water and drying under airflow, electrodes were incubated with 10 μL of a mixture solution containing 0.4 M EDC and 0.1 M Sulfo-NHS in 25 mM MES buffer, pH 5.0, for 35 minutes at room temperature in a humid chamber. Covalent attachment of CRP cAbs was carried out by drop casting 10 μL of anti-CRP solution (250 μg mL^{-1} in PBS, pH 7.4) and incubated at room temperature for 2.5 hours, followed by a 1-hour blocking step with 1.0% BSA prepared in PBS. Electrodes were stored in 1% BSA in PBS until use.

CRP detector antibody conjugation.

20 nm carboxylic acid functionalized PEGylated gold AuNPs were activated with EDC/Sulfo-NHS mix solution (30 mg mL^{-1} and 36 mg mL^{-1} respectively) in 10 mM MES buffer (pH 5.5) for 30 minutes. The conjugates were washed with 1X PBS containing 0.1% Tween® 20 (PBST) and centrifuged at 6500 relative centrifugal force (rcf) for 30 minutes. After supernatant removal, 50 μg mL^{-1} polystreptavidin R (PS-R) was added and allowed to crosslink for 1 hour at room temperature. Following centrifugation at 3500 rcf for 30 minutes and supernatant removal, 5 μg mL^{-1} biotinylated anti-CRP dAb in 1% BSA prepared in 1X PBS (pH 7.4) was incubated for 1 hour at room temperature. After another round of washing (centrifugation at 2000 rcf), the carboxyl groups of PS-R and dAb on AuNP were activated with EDC/Sulfo-NHS mix solution (30 mg mL^{-1} and 36 mg mL^{-1} respectively) in 10 mM MES buffer (pH 5.5) for 30 minutes. After the washing step using centrifugation at 1500 rcf, 100 μM thionine was incubated for 1 hour. The final conjugate was washed with PBST, centrifuged at 1250 rcf, reconstituted in 1% BSA and filtered through 0.2 μm syringe filter to remove all aggregates.

For direct redox probe conjugation to antibodies, 100 μg mL^{-1} dAb was buffer exchanged by concentrating with a 100K MWCO protein concentrator and reconstituted in 10 mM MES buffer (pH 5.5). The carboxyl groups of dAb were activated with EDC/Sulfo-NHS mix solution (30 mg mL^{-1} and 36 mg mL^{-1} respectively) in 10 mM MES buffer (pH 5.5) for 30 minutes in column. Following buffer exchange with 1X PBS (pH 7.4), 100 μM thionine was incubated for 1 hour. The final conjugate was buffer exchanged with PBS, reconstituted in 1% BSA, and filtered through 0.2 μm syringe filter to remove all aggregates.

Characterization of the biosensing method.

The morphology and material properties of the LEG-based CRP sensing electrodes before and after surface modification were characterized by focused ion beam-scanning electron microscopy (FIB-SEM) (FEI Nova 600 NanoLab), transmission electron microscopy (TEM) (TecnaiTF-20), Raman spectroscopy, x-ray photoelectron spectroscopy (XPS) (Kratos Ultra XPS), and Ultraviolet–visible spectroscopy (UV-vis). Raman spectra of the electrodes were recorded using a 532.8 nm laser with an inVia Reflex (Renishaw, UK). Dynamic light scattering data were collected with Malvern Dynamic Light Scattering (DLS) Zetasizer. UV-Vis absorbance data were collected with BioTek Synergy HTX multi-mode reader.

Author Manuscript Author Manuscript Author Manuscript Author Manuscript

In vitro electrochemical characterizations were carried out on a CHI660e electrochemical workstation with a commercial Ag/AgCl electrode as the reference electrode.

Specifically, in order to characterize surface modification after each step electrochemically, differential pulse voltammetry (DPV) and open circuit potential-electrochemical impedance spectroscopy (OCP-EIS) readings were obtained in 0.1M KCl, containing 5.0 mM of $K_4Fe(CN)_6/K_3Fe(CN)_6$ (1:1) under conditions: potential range, −0.2–0.6 V; pulse width, 0.2 s; incremental potential, 4 mV; amplitude, 50 mV; frequency range, 0.1–10^6 Hz; amplitude, 5 mV.

Comparison of sensing performance with bare graphene-modified sensors was conducted following protocols published previously[43,61]. Briefly, the LEG electrodes were electrodeposited with poly(propionic acid) (PPA) *via* cyclic voltammetry or modified with pyrenebutyric acid (PBA) *via* π–π stacking by immersing the electrodes in 5 mM PBA prepared in DMF for 2 hours. LEG was electrochemically oxidized in PBS (1X, pH 3) at +1.75V for 45 seconds to produce graphene oxide (LEGO). Next the LEG electrodes were activated with EDC/Sulfo-NHS and were incubated with cAbs (250 μg mL^{-1} in PBS, pH 7.4) for 2.5 hours. To compare the electrochemical performance, the cAb-modified electrodes were incubated in 0 ng mL^{-1} or 10 ng mL^{-1} CRP in 1% BSA for 15 minutes, followed by for 15-minutes incubation in 1 μg mL^{-1} horseradish peroxidase (HRP) conjugated anti-CRP dAbs. Amperometric readings were recorded at 0 V in 50 mM sodium phosphate buffer (pH 6.0) containing 2.0 mM hydroquinone and 10 mM H_2O_2.

Electrochemical detection of CRP in buffer and biofluids was performed by mixing 4.5 μL-aliquots of CRP standards (or raw biofluids to be analyzed) with 0.5 μL dAb-loaded AuNPs (1/10 dilution prepared in 10% BSA prepared in 1X PBS, pH 7.4) and drop casting onto the working electrode, allowing CRP and dAb binding to take place for 15 minutes before rinsing with PBS. Square wave voltammetry (SWV) was used to record the CRP signal in 1X PBS, pH 7.4. SWV conditions: potential range, 0–-0.6 V; increment potential, 10 mV; amplitude, 50 mV; frequency, 25 Hz. The performance of the CRP sensors subjected to different incubation and detection conditions was evaluated from pH 6 to pH 10 and from 0.1X PBS to 2X PBS. Selectivity test was conducted in the presence of mixture solutions of 1/100 dAb-loaded AuNPs (final concentration) and 5 ng mL^{-1} cortisol, immunoglobulin G (IgG), tumor necrosis factor alpha (TNF-α) and CRP in the presence of 5 ng mL^{-1} CRP.

The influence of mechanical deformation on the sensor performance was investigated by incubating the sensor patch in CRP standards for 15 minutes or McIlvaine buffers for pH sensors under mechanical deformation (with radii of bending curvature 2.5 and 3.5 cm). The temperature sensor readings were recorded by placing the patch in an oven under mechanical deformation.

Evaluation of the microfluidic module.

The microfluidic module was evaluated with both numerical simulation and experimental flow tests.

Author Manuscript Author Manuscript Author Manuscript Author Manuscript

Numerical simulation.—Simulation of the CRP-antibody bonding reaction and mass transport process were conducted using the commercial software COMSOL Multiphysics through finite element analysis (FEA). Tetrahedral elements with refined meshes allowed modeling of the source diffusion in 3D space with testified accuracy. The chemical reaction rate is described by law of mass action

$$r = k^f c_{CRP} \cdot c_{antibody} - k^r c_{complex}$$

Where r, k^f, k^r, c_{CRP}, $c_{antibody}$, and $c_{complex}$ denote reaction rate, forward reaction coefficient, reverse reaction coefficient, concentration of CRP, concentration of antibody and concentration of CRP-antibody complex, respectively. The forward and reverse reaction coefficients are assumed to be 5.96×10^4 $M^{-1}s^{-1}$ and 2.48×10^{-3} s^{-1}, respectively[62]. The concentration of CRP in sweat is assumed to be 1 ng mL^{-1}.

The fluid behavior is described by the Navier-Stokes equation for incompressible flow

$$\rho\left(\frac{\partial v}{\partial t} + (v \cdot \nabla)v\right) = -\nabla p + \mu \nabla^2 v$$

$$\nabla \cdot v = 0$$

Where ρ, v, p, and μ denote liquid density, flow velocity, pressure, and viscosity, respectively. The sweat flow rate is 1.5 μg mL^{-1}. And the convection diffusion is described by

$$\frac{\partial c}{\partial t} + v \cdot \nabla c = D \nabla^2 c$$

Where c and D denote concentration and diffusion coefficient. The diffusion coefficient of CRP is 5×10^{-11} $m^{-2}s^{-1}$, the diffusion coefficient of antibody and CRP-antibody complex are set to be the same as gold nanoparticles which is 1×10^{-12} $m^{-2}s^{-1}$.

Experimental flow tests.—The flow tests to evaluate the microfluidic sensing system were done with a syringe pump (Thermo Fisher Scientific, 78–01001). For the fluorescent flow test, a flow patch was pre-deposited with 0.5 μg Peridinin-Chlorophyll Protein Complex (PerCP) and 200 μg BSA in the reagent reservoir and dried before full patch assembly, and 0.25 μg mL^{-1} FITC-albumin in 1X PBS was injected into the patch placed on a blue light transilluminator (Accuris SmartBlue Mini) at a flow rate of 1.5 μL min^{-1}. For the CRP sensor validation, 7 μL of 2X PBS and 2 μL of 10X dAb-loaded AuNP were deposited in the reagent reservoir and dried before full patch assembly, artificial sweat (0.1X or 0.2X PBS) containing CRP (1 ng mL^{-1} or 5 ng mL^{-1}) was injected into the patch at specified flow rate. For on-body flow test, an assembled flow patch pre-deposited with black dye in the reagent reservoir was attached onto a subject's arm after sweat induction by iontophoresis.

Author Manuscript Author Manuscript Author Manuscript Author Manuscript

Electronic system design and integration.

A 2-layer flexible printed circuit board (FPCB) was designed using Eagle CAD and Fusion 360. The FPCB outline was designed as a rounded rectangle (31.7 mm × 25.5 mm) the same size as the microfluidic sensor patch such that the patch can be inserted directly underneath the FPCB via a cutout (10 mm × 3.8 mm). The electronic system is composed of a magnetic reed switch (MK24-B-3, Standex-Meder Electronics) and a voltage regulator (ADP162, Analog Devices) for power management; a boost converter (TPS61096, Texas Instruments), BJT array (BCV62C, Nexperia), and analog switch (DG468, Vishay Intertechnology) for iontophoretic induction; an electrochemical front-end (AD5941, Analog Devices), an operational amplifier (LPV811, Texas Instruments), and a voltage divider for sensor array interface; and a Bluetooth Low Energy (BLE) module (CYBLE-222014–01, Cypress Semiconductor) programmed via PSoC Creator 4.3 for system control and Bluetooth wireless communication. A BLE dongle (CY5677, Cypress Semiconductor) programmed via PSoC Creator 4.3 or custom mobile application programmed via Flutter was used to establish a BLE connection with the wearable device and to wirelessly acquire sensor data for calibration and voltammogram analysis. A rechargeable 3.8 V lithium button cell battery with capacity of 8 mAh was used to power the electronic system. To reduce the existing noise caused by motion artifacts, filtering and smoothing techniques are employed. On the hardware side, the electrochemical AFE filters noise from the ADC *via* digital filters. On the software side, smoothing algorithms (moving average filter/median filter) are automatically applied in real-time.

Subjects and procedures.

The performance of the wearable sensor was evaluated in human sweat and saliva samples from healthy human subjects and subjects recently recovered from COVID-19 infection in compliance with the protocols that were approved by the institutional review board (IRB) (#19–0892, #19–0894 and #21–1108) at California Institute of Technology (Caltech). The participating subjects were recruited from Caltech campus and the neighboring communities through advertisement by posted notices, word of mouth, and email distribution. All subjects gave written, informed consent before participation in the study.

Human subjects for evaluation of the sweat CRP in COPD monitoring were recruited at The Lundquist Institute/Harbor-UCLA Medical Center with the protocol approved by the IRB at the Lundquist Institute (#32051–01). Male and female, current or former smokers with or without COPD were recruited. Inclusion criteria were: aged 40–80 years; BMI between 18–40 kg m^{-2}; >10 pack-year smoking history. Additional inclusion criteria for COPD patients were: forced expiratory volume in 1 second / forced vital capacity (FEV_1/FVC) <0.7; FEV_1 < 80%; modified Medical Research Council (mMRC) dyspnea scale ≥2; COPD Assessment Test (CAT) >5. Exclusion criteria included: significant chronic disease, other than COPD; severe and/or uncontrolled medical conditions that could interfere with the study; malignancy within the previous 2 years; HIV infection; active tuberculosis; documented cardiovascular disease or resting ECG abnormality; use of systemic corticosteroids; COPD exacerbation within 3 months; those requiring supplemental oxygen.

Author Manuscript Author Manuscript Author Manuscript Author Manuscript

Adult patients with a diagnosis of heart failure were recruited from the University of California, Los Angeles (UCLA) Ahmanson Cardiomyopathy Clinic, and the protocol was approved by the UCLA IRB (#19–000388). Exclusion criteria included pregnancy, severe skin allergy, current need for inpatient hospitalization, current use of beta-blocker medication therapy due to theoretical interaction with pilocarpine, active inotropic medication infusion, hypotension or hypertension, severe bradycardia or tachycardia, or significant cardiac conduction disorder.

Human subjects for evaluation of the sweat CRP in infection monitoring were recruited with a protocol approved by the IRB at Cedars-Sinai Medical Center (#STUDY00001099). Enrolled patients were admitted to the hospital ≥18 years of age that had an active infection (e.g., pneumonia, UTI, cellulitis, etc.).

Sample collection for in vitro studies.—An iontophoresis session was implemented using a Model 3700 Macroduct Sweat Collection System for sweat induction, the subjects were asked to wear a Macroduct collector over a period of 60 minutes for sweat collection. Subjects were asked to refrain from eating, drinking, and chewing gum 30 minutes before saliva collection. After rinsing mouth with water, volunteers deposited saliva in 1.5 mL Eppendorf tubes which were subsequently centrifuged at 10000 revolutions per minute (rpm) for 10 minutes and analyzed. Fresh blood samples were collected at same periods of time as saliva and/or sweat either using a finger-prick approach or *via* venous blood draw. Once standardized clotting procedure finished, serum was separated by centrifuging at 3575 rpm for 15 minutes, and instantly stored at −80 °C.

Human sample analysis with enzyme-linked immunosorbent assay (ELISA).—ELISA tests for CRP were performed in an accuSkan™ FC Filter-Based Microplate Photometer at a detection wavelength of 450 nm, according to the manufacturer's instructions. Briefly, 96-well Nunc MaxiSorp™ flat-bottom plate was modified with anti-CRP antibodies in 50 mM carbonate buffer (pH 9.6) overnight at 4°C. Standards or diluted biofluid samples prepared in 1% BSA were added to anti-CRP antibody-coated microtiter plate wells and incubated for 2 hours at room temperature. After three washing steps with wash buffer (PBST, pH7.4), biotinylated detector antibodies were added to each well and incubated for 2 hours at room temperature. After three washing steps, streptavidin-HRP was added and incubated for 20 minutes a room temperature. Following three washing steps, 100 μL of 3,3′,5,5′-Tetramethylbenzidine (TMB) substrate was incubated for 15 minutes, and absorbance values were measured immediately after the addition of 50 μL of 1M H_2SO_4 to each well.

Human sample analysis with liquid chromatography-tandem mass spectrometry (LC-MS/MS).—1 mL pooled sweat sample was concentrated using Amicon centrifugal filters with a molecular weight cutoff (MWCO) of 3 kDa to 15 μL final volume at a concentration factor of 67X. The concentrated samples were buffer exchanged in 8 M urea in 10 mM 4-(2-hydroxyethyl)-1-piperazineethanesulfonic acid (HEPES) buffer (pH 7.4), reduced with 3.7 mM tris(2-carboxyethyl)phosphine (TCEP) for 20 minutes at 37 °C and alkylated with 10 mM chloroacetamide (CAA) for 15 minutes at 37 °C. Proteins from each sample were digested at 37 °C lysyl endopeptidase at a 1:100 ratio for 2 hours.

Author Manuscript Author Manuscript Author Manuscript Author Manuscript

The samples were then diluted with 50 mM HEPES buffer (pH 7.4) to a final concentration of 2 M urea and digested with trypsin at a 1:50 ratio at 37 °C for 14 hours. Digested peptides were acidified with 20% trifluoroacetic acid (TFA) and desalted with C18 spin columns using 50% acetonitrile (ACN) as the activation solution, 0.5% TFA in 5% ACN as the equilibration solution and wash solution, 2% TFA in 20% ACN as the sample buffer, and 0.2% formic acid (FA) in 70% ACN as the elution buffer. Desalted peptides were freeze-dried and stored at −20 °C until use. Lyophilized peptide was reconstituted in 10 μL 0.2% FA in 2% ACN. All incubation procedures were carried out with shaking at 750 rpm in the dark.

LC-MS/MS analysis was performed with an Vanquish Neo UHPLC system (ThermoFisher Scientific, San Jose, CA) coupled to an Orbitrap Eclipse Tribrid mass spectrometerer (ThermoFisher Scientific, San Jose, CA). Peptides were separated on an Aurora UHPLC Column (25 cm × 75 μm, 1.6 μm C18, AUR2–25075C18A, Ion Opticks) with a flow rate of 0.35 μL min^{-1} for a total duration of 75 min and ionized at 1.6 kV in the positive ion mode. The gradient was composed of 6% solvent B (3.5 min), 6–25% B (41.5 min), 25–40% B (15 min), 40–98% B (1 min) and 98% B (14 min); solvent A: 0.1% FA in water; solvent B: 80% ACN and 0.1% FA. MS1 scans were acquired at the resolution of 120,000 from 350 to 1,800 m z^{-1}, AGC target 1e6, and maximum injection time 50 ms. The charge states and intensity threshold of precursor ions for triggering MS2 was set to 2–7 and 5e3, respectively. For targeted CRP analysis, the precursor ions from the inclusion list (Supplementary Table 1) were selected for MS2 spectrum acquisition in the ion trap using fast scan rate and quadrupole isolation mode (isolation window: 1.2 m z^{-1}) with higher-energy collisional dissociation (HCD, 30%) activation type. Dynamic exclusion was set to 30 s. The temperature of ion transfer tube was 300°C and the S-lens radio frequency (RF) level was set to 30. MS2 fragmentation spectra were searched with Proteome Discoverer SEQUEST (version 2.5, Thermo Scientific) against in silico tryptic digested Uniprot Human database. The maximum missed cleavages was set to 2. Dynamic modifications were set to oxidation on methionine (M, +15.995 Da), protein N-terminal acetylation (+42.011 Da) and Met-loss (−131.040 Da). Carbamidomethylation on cysteine residues (C, +57.021 Da) was set as a static modification. The maximum parental mass error was set to 10 ppm, and the MS2 mass tolerance was set to 0.6 Da. The false discovery threshold was set strictly to 0.01 using the Percolator Node validated by q-value. The relative abundance of parental peptides was calculated by integration of the area under the curve of the MS1 peaks using the Minora label-free quantification (LFQ) node.

On-body wearable evaluation.—The subjects' arm was cleaned with alcohol swabs and gauze before the wearable sensor patches were placed on the body. A 5-min iontophoresis was applied to the subject. During the on-body trial, the data from the sensor patches were wirelessly sent to the user interface *via* Bluetooth. The sensor system continuously acquired and transmitted impedance data from the ionic strength sensors. When the impedance data plateaued after an increase, the system would proceed with an SWV scan over the CRP sensor followed by the acquisition of the readings of pH and skin temperature sensors. After being real-time calibrated using simultaneously collected electrolyte and pH information, the acquired data was converted to the concentration levels based on the calibration curve.

Author Manuscript Author Manuscript Author Manuscript Author Manuscript

Reporting Summary.

Further information on research design is available in the Nature Research Reporting Summary linked to this article.

Supplementary Material

Refer to Web version on PubMed Central for supplementary material.

Acknowledgement

This project was supported by the American Heart Association grant 19TPA34850157, National Institutes of Health grants R01HL155815 and R21DK13266, National Science Foundation grant 2145802, Office of Naval Research grants N00014-21-1-2483 and N00014-21-1-2845, High Impact Pilot Research Award T31IP1666 from the Tobacco-Related Disease Research Program, Sloan Research Fellowship, and the Technology Ventures Internal Project Fund at Cedars-Sinai. J.T. was supported by the National Science Scholarship (NSS) from the Agency of Science Technology and Research (A*STAR) Singapore. E.D. was supported by National Institutes of Health grant T32EB027629. We gratefully acknowledge critical support and infrastructure provided for this work by the Kavli Nanoscience Institute at Caltech. We acknowledge support from the Beckman Institute of the California Institute of Technology to the Molecular Materials Research Center and Jake Evans for help with XPS. The Proteome Exploration Laboratory (PEL) is supported by the Beckman Institute and NIH 1S10OD02001301. We thank George R. Rossman for assistance in Raman Spectroscopy. We also thank Emad Bayoumi; Ethan Pascual; Po-En (“Ann”) Chen at Cedars-Sinai Medical Center for their assistance for human subject recruiting. We thank Rebeca M. Torrente-Rodríguez for constructive feedback on manuscript preparation.

Data availability

The main data supporting the results in this study are available within the paper and its Supplementary Information. Source data for Figs. 3 and 5 are provided with this paper. All raw and analysed datasets generated during the study are available from the corresponding author on request.

References

1. The top 10 causes of death https://www.who.int/news-room/fact-sheets/detail/the-top-10-causes-of-death.
2. Mannino DM et al. Economic burden of COPD in the presence of comorbidities. Chest 148, 138–150 (2015). [PubMed: 25675282]
3. Ferrucci L & Fabbri E Inflammageing: chronic inflammation in ageing, cardiovascular disease, and frailty. Nat. Rev. Cardiol 15, 505–522 (2018). [PubMed: 30065258]
4. Ashley NT, Weil ZM & Nelson RJ Inflammation: mechanisms, costs, and natural variation. Annu. Rev. Ecol. Evol. Syst 43, 385–406 (2012).
5. Schett G & Neurath MF Resolution of chronic inflammatory disease: universal and tissue-specific concepts. Nat. Commun 9, 3261 (2018). [PubMed: 30111884]
6. Furman D et al. Chronic inflammation in the etiology of disease across the life span. Nat. Med 25, 1822–1832 (2019). [PubMed: 31806905]
7. Wylezinski LS, Gray JD, Polk JB, Harmata AJ & Spurlock CF Illuminating an invisible epidemic: a systemic review of the clinical and economic benefits of early diagnosis and treatment in inflammatory disease and related syndromes. J. Clin. Med 8, 493 (2019). [PubMed: 30979036]
8. The Emerging Risk Factors Collaboration, et al. C-reactive protein concentration and risk of coronary heart disease, stroke, and mortality: an individual participant meta-analysis. Lancet 375, 132–140 (2010). [PubMed: 20031199]
9. Ridker PM A test in context: high-sensitivity C-reactive protein. J. Am. Coll. Cardiol 67, 712–723 (2016). [PubMed: 26868696]

Author Manuscript Author Manuscript Author Manuscript Author Manuscript

10. Proctor MJ et al. Systemic inflammation predicts all-cause mortality: a glasgow inflammation outcome study. PLoS One 10, e0116206 (2015). [PubMed: 25730322]
11. Prins BP et al. Investigating the causal relationship of C-reactive protein with 32 complex somatic and psychiatric outcomes: A large-scale cross-consortium mendelian randomization study. PLOS Med 13, e1001976 (2016). [PubMed: 27327646]
12. Balayan S, Chauhan N, Rosario W & Jain U Biosensor development for C-reactive protein detection: A review. Appl. Surf. Sci. Adv 12, 100343 (2022).
13. Young B, Gleeson M & Cripps AW C-reactive protein: a critical review. Pathology 23, 118–124 (1991). [PubMed: 1720888]
14. Lobo SM Sequential C-reactive protein measurements in patients with serious infections: does it help? Crit. Care 16, 130 (2012). [PubMed: 22731851]
15. Guo S, Mao X & Liang M The moderate predictive value of serial serum CRP and PCT levels for the prognosis of hospitalized community-acquired pneumonia. Respir. Res 19, 193 (2018). [PubMed: 30285748]
16. Gao W et al. Fully integrated wearable sensor arrays for multiplexed in situ perspiration analysis. Nature 529, 509–514 (2016). [PubMed: 26819044]
17. Yang Y & Gao W Wearable and flexible electronics for continuous molecular monitoring. Chem. Soc. Rev 48, 1465–1491 (2019). [PubMed: 29611861]
18. Ray TR et al. Soft, skin-interfaced sweat stickers for cystic fibrosis diagnosis and management. Sci. Transl. Med 13, eabd8109 (2021).
19. Kim J, Campbell AS, de Ávila BE-F & Wang J Wearable biosensors for healthcare monitoring. Nat. Biotechnol 37, 389–406 (2019). [PubMed: 30804534]
20. Lee H et al. A graphene-based electrochemical device with thermoresponsive microneedles for diabetes monitoring and therapy. Nat. Nanotech 11, 566–572 (2016).
21. Koh A et al. A soft, wearable microfluidic device for the capture, storage, and colorimetric sensing of sweat. Sci. Transl. Med 8, 366ra165 (2016).
22. Ates HC et al. On-site therapeutic drug monitoring. Trends Biotech 38, 1262–1277 (2020).
23. Bariya M, Nyein HYY & Javey A Wearable sweat sensors. Nat. Electron 1, 160–171 (2018).
24. Parlak O, Keene ST, Marais A, Curto VF & Salleo A Molecularly selective nanoporous membrane-based wearable organic electrochemical device for noninvasive cortisol sensing. Sci. Adv 4, eaar2904 (2018).
25. Tu J, Torrente-Rodríguez RM, Wang M & Gao W The era of digital health: A review of portable and wearable affinity biosensors. Adv. Funct. Mater 30, 1906713 (2020).
26. Heikenfeld J et al. Accessing analytes in biofluids for peripheral biochemical monitoring. Nat. Biotechnol 37, 407–419 (2019). [PubMed: 30804536]
27. Yang Y et al. A laser-engraved wearable sensor for sensitive detection of uric acid and tyrosine in sweat. Nat. Biotechnol 38, 217–224 (2020). [PubMed: 31768044]
28. Yu Y et al. Biofuel-powered soft electronic skin with multiplexed and wireless sensing for human-machine interfaces. Sci. Robot 5, eaaz7946 (2020).
29. Sempionatto JR et al. An epidermal patch for the simultaneous monitoring of haemodynamic and metabolic biomarkers. Nat. Biomed. Eng 5, 737–748 (2021). [PubMed: 33589782]
30. Emaminejad S et al. Autonomous sweat extraction and analysis applied to cystic fibrosis and glucose monitoring using a fully integrated wearable platform. Proc. Natl. Acad. Sci. USA 114, 4625–4630 (2017). [PubMed: 28416667]
31. Bandodkar AJ, Jeang WJ, Ghaffari R & Rogers JA Wearable sensors for biochemical sweat analysis. Annual Rev. Anal. Chem 12, 1–22 (2019).
32. Xuan X, Pérez-Ràfols C, Chen C, Cuartero M & Crespo GA Lactate biosensing for reliable on-body sweat analysis. ACS Sens 6, 2763–2771 (2021). [PubMed: 34228919]
33. Pirovano P et al. A wearable sensor for the detection of sodium and potassium in human sweat during exercise. Talanta 219, 121145 (2020). [PubMed: 32887090]
34. Garcia-Cordero E et al. Three-dimensional integrated ultra-low-volume passive microfluidics with ion-sensitive field-effect transistors for multiparameter wearable sweat analyzers. ACS Nano 12, 12646–12656 (2018). [PubMed: 30543395]

Author Manuscript Author Manuscript Author Manuscript Author Manuscript

35. He W et al. Integrated textile sensor patch for real-time and multiplex sweat analysis. Sci. Adv 5, eaax0649 (2019).
36. Choi D-H, Kitchen GB, Jennings MT, Cutting GR & Searson PC Out-of-clinic measurement of sweat chloride using a wearable sensor during low-intensity exercise. npj Digit. Med 3, 49 (2020). [PubMed: 32258431]
37. Zhong B, Jiang K, Wang L & Shen G Wearable sweat loss measuring devices: from the role of sweat loss to advanced mechanisms and designs. Adv. Sci 9, 2103257 (2022).
38. Lin H et al. A programmable epidermal microfluidic valving system for wearable biofluid management and contextual biomarker analysis. Nat. Commun 11, 4405 (2020). [PubMed: 32879320]
39. Saldanha DJ, Cai A & Dorval Courchesne N-M The evolving role of proteins in wearable sweat biosensors. ACS Biomater. Sci. Eng 9, 2020–2047 (2021). [PubMed: 34491052]
40. Mishra RK et al. Continuous opioid monitoring along with nerve agents on a wearable microneedle sensor array. J. Am. Chem. Soc 142, 5991–5995 (2020). [PubMed: 32202103]
41. Wang B et al. Wearable aptamer-field-effect transistor sensing system for noninvasive cortisol monitoring. Sci. Adv 8, eabk0967 (2022).
42. An JE et al. Wearable cortisol aptasensor for simple and rapid real-time monitoring. ACS Sens 7, 99–108 (2022). [PubMed: 34995062]
43. Torrente-Rodríguez RM et al. Investigation of cortisol dynamics in human sweat using a graphene-based wireless mHealth system. Matter 2, 921–937 (2020). [PubMed: 32266329]
44. Jagannath B et al. Novel approach to track the lifecycle of inflammation from chemokine expression to inflammatory proteins in sweat using electrochemical biosensor. Adv. Mater. Technol 7, 2101356 (2022).
45. Gao Y et al. A flexible multiplexed immunosensor for point-of-care in situ wound monitoring. Sci. Adv 7, eabg9614 (2021).
46. Barkas F, Liberopoulos E, Kei A & Elisaf M Electrolyte and acid-base disorders in inflammatory bowel disease. Ann. Gastroenterol 26, 23–28 (2013). [PubMed: 24714322]
47. Majewski S et al. Skin condition and its relationship to systemic inflammation in chronic obstructive pulmonary disease. Int. J. Chron. Obstruct. Pulmon. Dis 12, 2407–2415 (2017). [PubMed: 28860735]
48. Yang X et al. Graphene uniformly decorated with gold nanodots: in situ synthesis, enhanced dispersibility and applications. J. Mater. Chem 21, 8096–8103 (2011).
49. Yu Y et al. All-printed soft human-machine interface for robotic physicochemical sensing. Sci. Robot 7, eabn0495 (2022).
50. Harshman SW et al. The proteomic and metabolomic characterization of exercise-induced sweat for human performance monitoring: A pilot investigation. PLoS One 13, e0203133 (2018). [PubMed: 30383773]
51. Pinto-Plata VM et al. C-reactive protein in patients with COPD, control smokers and non-smokers. Thorax 61, 23–28 (2006). [PubMed: 16143583]
52. Retamales I et al. Amplification of inflammation in emphysema and its association with latent adenoviral infection. Am. J. Respir. Crit. Care Med 164, 469–473 (2001). [PubMed: 11500352]
53. Tonstad S & Cowan JL C-reactive protein as a predictor of disease in smokers and former smokers: a review. Int. J. Clin. Pract 63, 1634–1641 (2009). [PubMed: 19732183]
54. Simmonds SJ, Cuijpers I, Heymans S & Jones EAV Cellular and molecular differences between HFpEF and HFrEF: a step ahead in an improved pathological understanding. Cells 9, 242 (2020). [PubMed: 31963679]
55. Lakhani I et al. Diagnostic and prognostic value of serum C-reactive protein in heart failure with preserved ejection fraction: a systematic review and meta-analysis. Heart Fail. Rev 26, 1141–1150 (2021). [PubMed: 32030562]
56. Butler J et al. Clinical and economic burden of chronic heart failure and reduced ejection fraction following a worsening heart failure event. Adv. Ther 37, 4015–4032 (2020). [PubMed: 32761552]
57. Albar Z et al. Inflammatory markers and risk of heart failure with reduced to preserved ejection fraction. Am. J. Cardiol 167, 68–75 (2022). [PubMed: 34986991]

Author Manuscript Author Manuscript Author Manuscript Author Manuscript

58. Xin Y, Zhou J, Nesser H & Lubineau G Design strategies for strain-Insensitive wearable healthcare sensors and perspective based on the seebeck coefficient. Adv. Electron. Mater 9, 2200534 (2023).

59. Wang M et al. A wearable electrochemical biosensor for the monitoring of metabolites and nutrients. Nat. Biomed. Eng 6, 1225–1235 (2022). [PubMed: 35970928]

60. Bandodkar AJ et al. Battery-free, skin-interfaced microfluidic/electronic systems for simultaneous electrochemical, colorimetric, and volumetric analysis of sweat. Sci. Adv 5, eaav3294 (2019).

61. Torrente-Rodríguez RM et al. SARS-CoV-2 RapidPlex: A graphene-based multiplexed telemedicine platform for rapid and low-cost COVID-19 diagnosis and monitoring. Matter 3, 1981–1998 (2020). [PubMed: 33043291]

62. Zhuang G, Katakura Y, Omasa T, Kishimoto M & Suga K-I Measurement of association rate constant of antibody-antigen interaction in solution based on enzyme-linked immunosorbent assay. J. Biosci. Bioeng 92, 330–336 (2001). [PubMed: 16233106]

Author Manuscript Author Manuscript Author Manuscript Author Manuscript

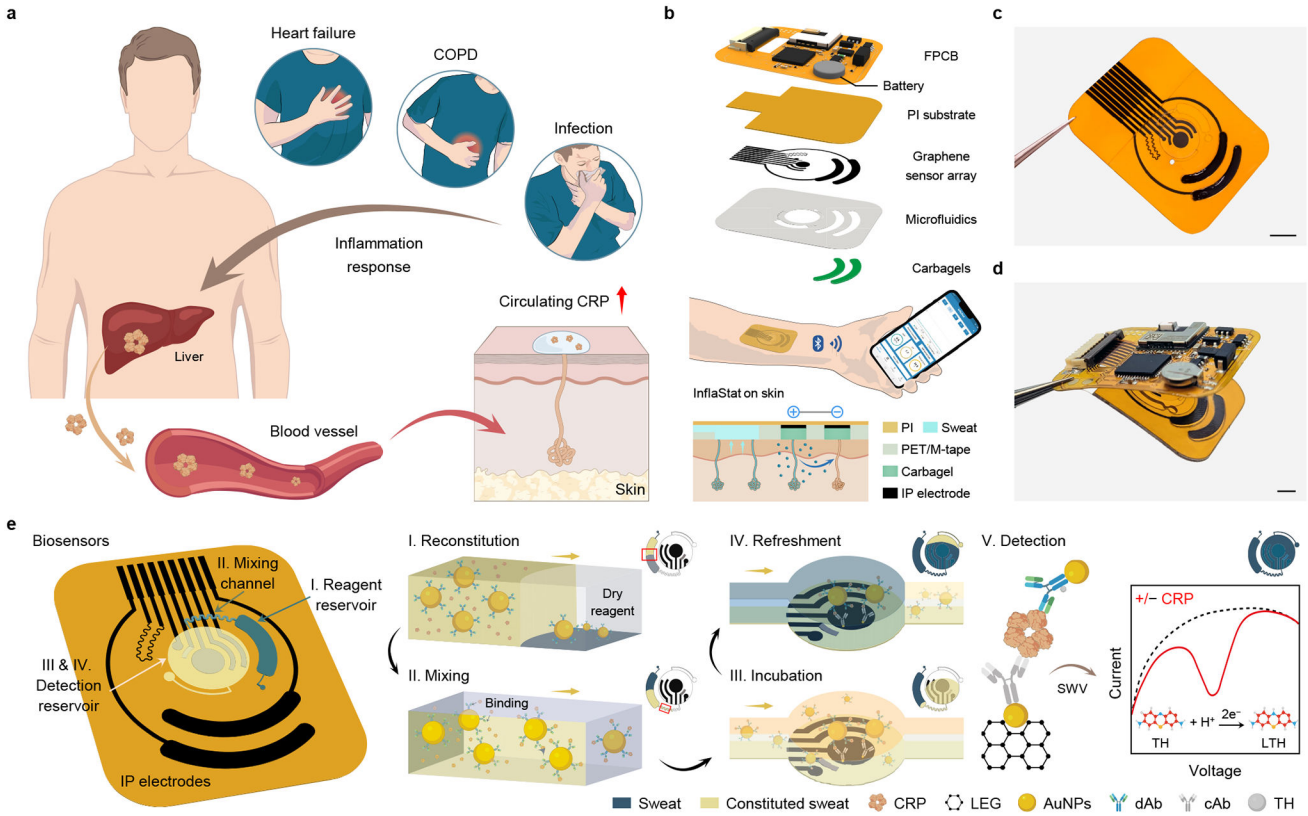

Fig. 1 |. Wearable electrochemical nanobiosensor for automatic, non-invasive, and wireless inflammation monitoring.

a, Circulating C-reactive protein (CRP), released from inflammatory responses, is closely related to various chronic and acute health conditions and could be secreted *via* the sweat gland. COPD, chronic obstructive pulmonary disease. **b,** Schematic of the skin-interfaced multimodal wearable nanobiosensor that contains an iontophoretic module for localized sweat extraction on-demand, a microfluidic module for automated sweat sampling and reagent routing, and a flexible laser-engraved graphene (LEG) multimodal sensor array for multiplexed sensing of sweat CRP, pH, temperature, and ionic strength. PI, polyimide; carbagel, carbachol hydrogel; PET/M-tape, polyethylene terephthalate/medical tape; IP, iontophoresis. **c,d,** Optical images of a disposable microfluidic graphene sensor patch (**c**) and a vertical stack assembly of the fully integrated wireless wearable system (**d**). Scale bars, 0.5 cm. **e,** The mechanism of *in situ* microfluidic sweat CRP analysis that involves fully-automatic sweat sampling, reagent routing, and detection. AuNPs, gold nanoparticles; cAb, capture antibody; dAb, detector antibody; SWV, square wave voltammetry; TH, thionine; LTH, leuco thionine.

Author Manuscript Author Manuscript Author Manuscript Author Manuscript

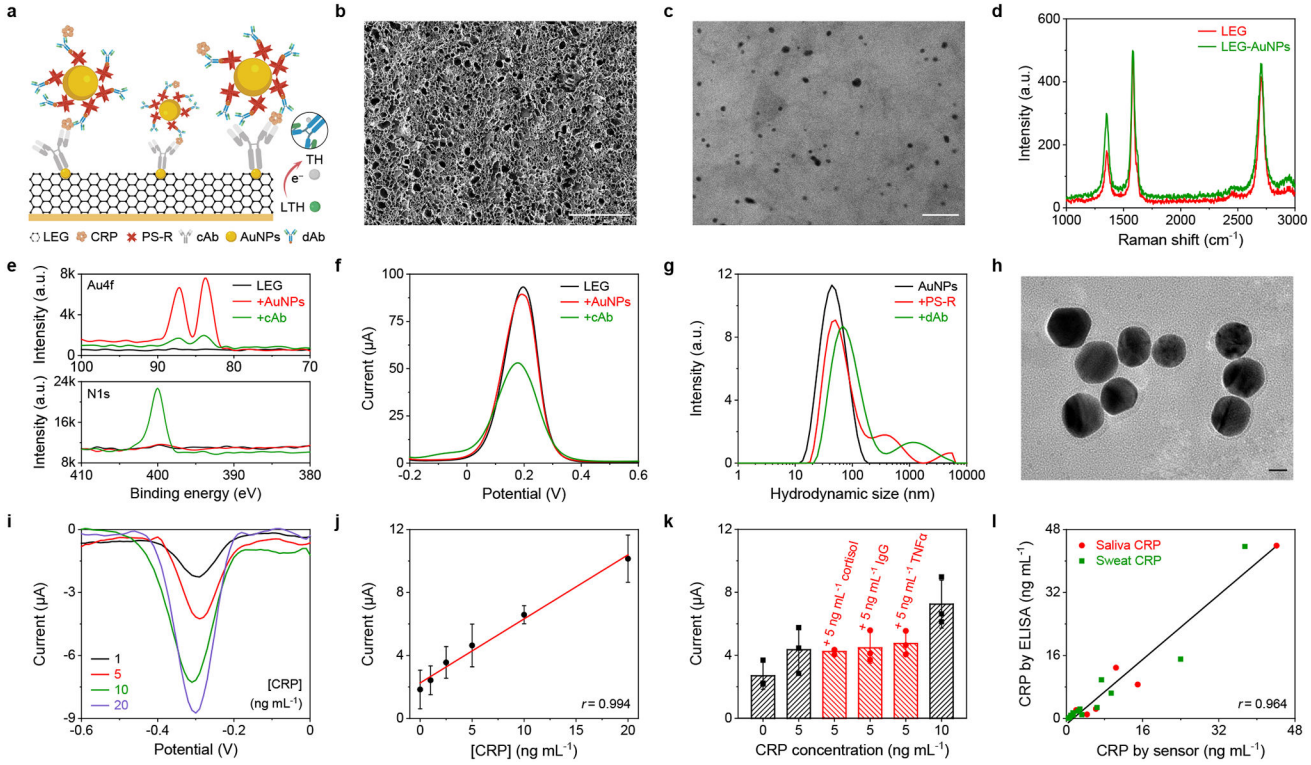

Fig. 2 |. Materials and electrochemical characterizations of the LEG-AuNPs CRP sensor. **a,** Schematic of the one-step electrochemical sandwich CRP immunosensor. PS-R, Polystreptavidin R. **b,** Scanning electron microscope (SEM) image of the mesoporous LEG electrode. Scale bar, 100 μm. **c,** Transmission electron microscopy (TEM) image of AuNPs-decorated graphene flakes. Scale bar, 50 nm. **d,** Raman spectra of LEG electrode and AuNPs-decorated LEG electrode. **e,** X-ray photoelectron spectra of the LEG after the deposition of AuNPs, thiol-based self-assembled monolayer (SAM), and cAb immobilization. **f,** DPV voltammograms of a sensing electrode in a 0.1 M KCl solution containing 5.0 mM $K_4Fe(CN)_6/K_3Fe(CN)_6$ (1:1) after each surface-modification step: bare LEG, deposition of AuNPs, SAM modification, carboxylic acid group activation with N-(3-Dimethylaminopropyl)-N'-ethylcarbodiimide/N-hydroxysulfosuccinimide (EDC/Sulfo-NHS), and cAb immobilization followed by bovine serum albumin (BSA) blocking. **g,** Hydrodynamic sizes of the PEGylated AuNPs after each conjugation step by dynamic light scattering: PS-R immobilization, biotinylated dAb binding, and redox molecule TH conjugation followed by BSA deactivation. **h,** TEM image of the dispersed dAb-loaded AuNPs with protein corona shells. Scale bar, 10 nm. **i,j,** SWV voltammograms (**i**) and the corresponding calibration plot (**j**) of the CRP sensors in 1X PBS (pH 7.4) with 0–20 ng mL^{-1} CRP and 1% BSA. Error bars represent the s.d. of the mean from 3 sensors. **k,** Selectivity of the CRP sensor to potential interferences in sweat. Error bars represent the s.d. of the mean from 3 sensors. **i,** Validation of the CRP sensor in human sweat samples (n=13 biological replicates) and saliva samples (n=6 biological replicates) with ELISA. The Pearson correlation coefficient was acquired through linear regression.

Author Manuscript Author Manuscript Author Manuscript Author Manuscript

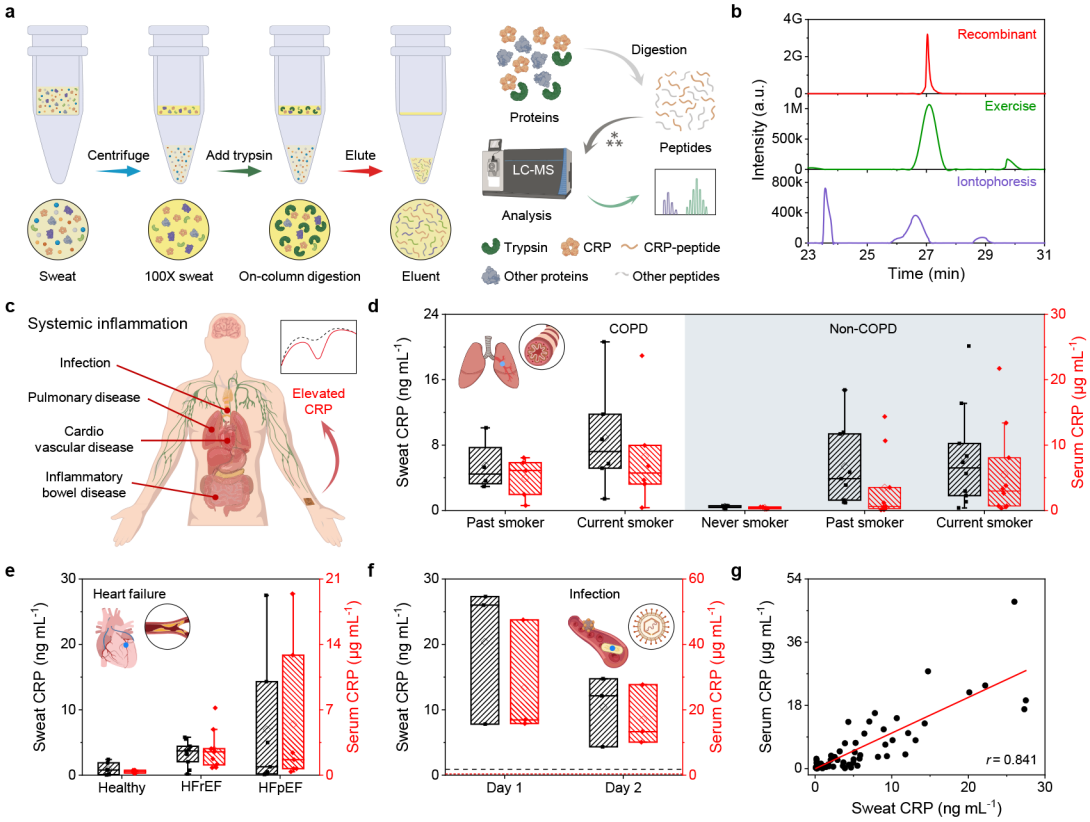

Fig. 3 |. Evaluation of sweat CRP for non-invasive monitoring of systemic inflammation in healthy and patient populations.

a, Schematic of proteomic analysis of human sweat using the liquid chromatography-mass spectrometry (LC-MS/MS). **b,** Chromatograms of the recombinant CRP reference peptide GYSIFSYATKR, iontophoresis-extracted and exercise sweat samples from human subjects. **c,** Schematic of the non-invasive inflammation monitoring in various health conditions with the LEG-AuNPs CRP sensor. **d,** Box-and-whisker plot of CRP levels in iontophoresis-extracted sweat and serum samples from subjects with COPD (n=10 biological replicates) and without COPD (n=24 biological replicates). The subjects are classified into five subgroups: current smokers with COPD (n=6 biological replicates) or without COPD (n=10 biological replicates), former smokers with COPD (n=4 biological replicates) and without COPD (n=9 biological replicates), and never smokers without COPD (n=5 biological replicates). The bottom whisker represents the minima; the top whisker represents the maxima; and the square in the box represents the mean. **e,** Box-and-whisker plot of CRP levels in sweat and serum samples from healthy subjects (n=7 biological replicates), patients with heart failure with reduced ejection fraction (HFrEF) (n=7 biological replicates), and patients with heart failure with preserved ejection fraction (HFpEF) (n=9 biological replicates). The bottom whisker represents the minima; the top whisker represents the maxima; the square in the box represents the mean. **f,** Box-and-whisker plot of CRP levels in sweat and serum samples from 3 patients with active infection on two consequent days (n=3 biological replicates). The bottom whisker represents the minima; the top whisker represents the maxima; the square in the box represents the mean. Dotted lines represent the mean

values of the sweat and serum CRP levels for healthy subjects. **g,** Correlation of serum and sweat CRP levels. The correlation coefficient *r* was acquired through Pearson's correlation analysis (n=80, p< .00001).

Author Manuscript Author Manuscript Author Manuscript Author Manuscript

Author Manuscript Author Manuscript Author Manuscript Author Manuscript

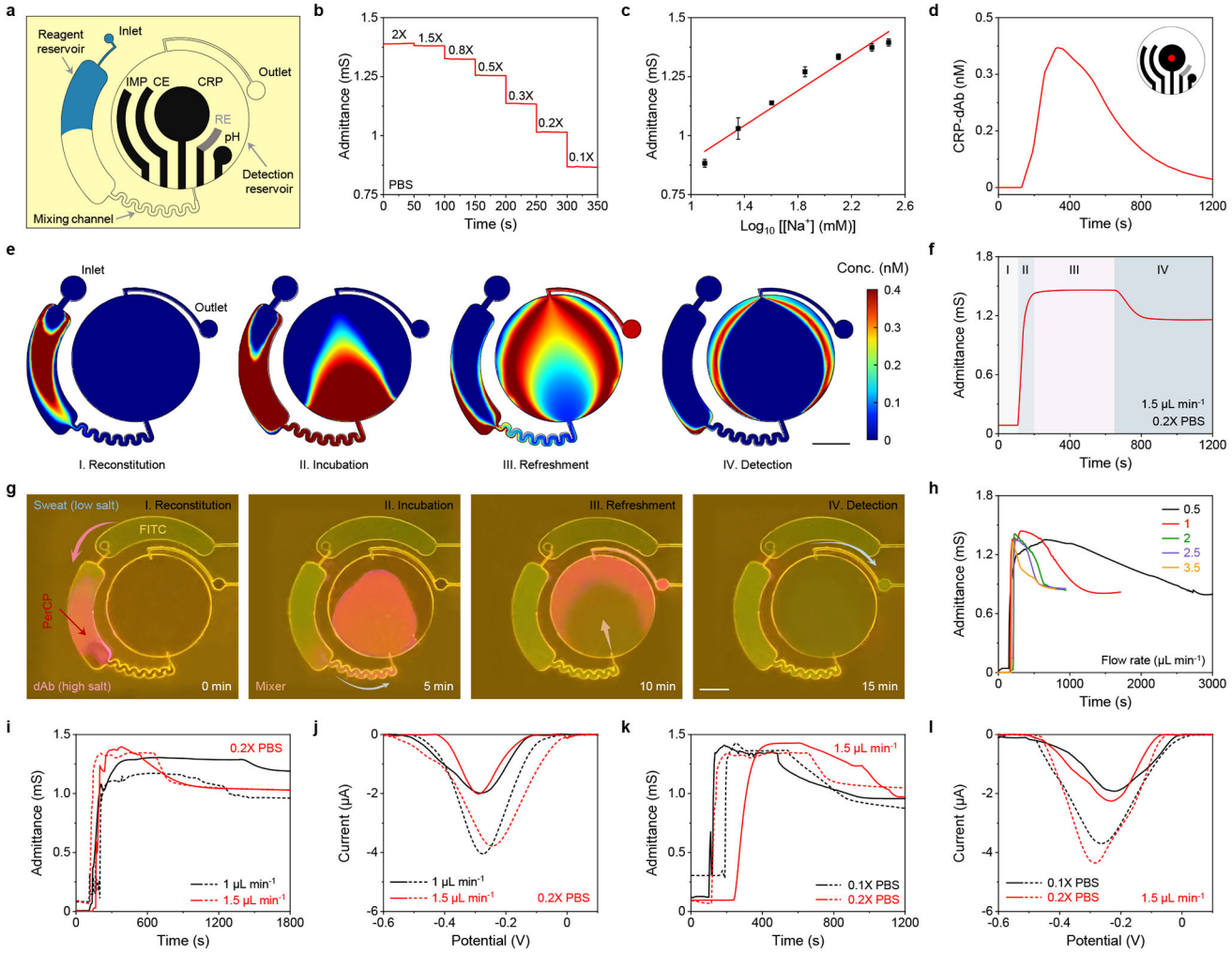

Fig. 4 |. Multiplexed microfluidic patch for automatic immunosensing.

a, Illustration of the multiplexed sensor array for automatic immunosensing. **b,c,** Admittance responses (**b**) and the corresponding calibration plot (**c**) of the impedimetric ionic strength sensor in NaCl solutions. Error bars represent the s.d. of the mean from 3 sensors. **d,** Simulated CRP-dAb concentration changes on the working electrode over time. Red dot in the inset image indicates the location of the concentration change plot. **e,** Simulated CRP-dAb concentrations colormaps showing phases of automatic sweat sampling and reagents routing toward *in situ* CRP detection: reconstitution (I), incubation (II), refreshment (III), and detection (IV). Scale bar, 200 μm. **f,g,** Admittance changes of the LEG ionic strength sensor (**f**) and optical images (**g**) during the four stages (I–IV) of automatic CRP sensing process in a laboratory flow test using artificial sweat (0.2X PBS) at a flow rate of 1.5 μL min^{-1}. Yellow fluorescein isothiocyanate (FITC)-albumin fluorescent label was used to imitate the flow of sweat CRP and red Peridinin Chlorophyll Protein Complex (PerCP) was used in place of dAb-loaded AuNPs. Scale bar, 200 μm. **h,** Admittance responses of the ionic strength sensor in artificial sweat (0.2X PBS) at different flow rates from 0.5 to 3.5 μL min^{-1}. **i–l,** Influence of the flow rates (**i,j**) and ionic strengths (**k,l**) on microfluidic

automatic CRP sensing. Solid and dotted lines represent tests performed in 1 and 5 ng mL^{-1} CRP, respectively.

Author Manuscript Author Manuscript Author Manuscript Author Manuscript

Author Manuscript Author Manuscript Author Manuscript Author Manuscript

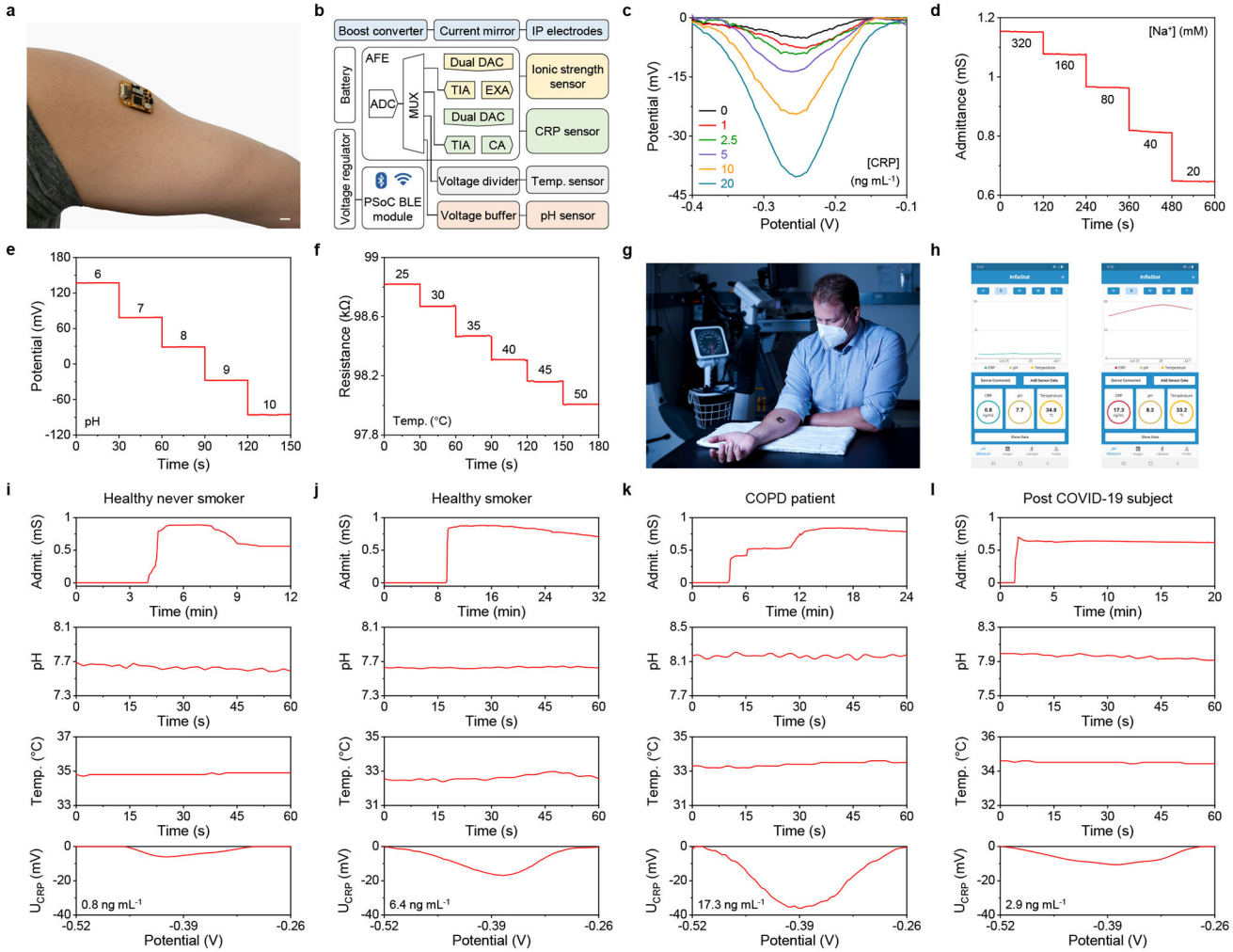

Fig. 5 |. On-body evaluation of the multiplexed wearable patch toward non-invasive automatic inflammation monitoring.

a, Image of a fully integrated wearable sensor on the arm of a human subject. Scale bar, 1 cm. **b,** Block diagram of the electronic system of the InflaStat. **c–f**, Calibration plots obtained using the wearable system from the CRP (**c**), ionic strength (**d**), pH (**e**) and temperature (**f**) sensors. Error bars represent the s.d. of the mean from 3 sensors. **g**, Photograph of a subject wearing the sensor patch during a clinical study. **h**, Custom mobile application for real-time data acquisition and display toward inflammation tracking. **i–l**, On-body multiplexed physicochemical analysis and CRP analysis with real-time sensor calibrations using the wearable sensor from a healthy never smoker (**i**), a healthy smoker (**j**), a COPD patient (**k**) and a post-COVID subject (**l**).